Published in final edited form as:
*Acta Biomater*. 2014 June ; 10(6): 2582–2590. doi:10.1016/j.actbio.2014.01.032.

# Interfibrillar shear stress is the loading mechanism of collagen fibrils in tendon

**Spencer E. Szczesny**[a] and **Dawn M. Elliott**[b,*]

[a]Department of Bioengineering, University of Pennsylvania, 240 Skirkanich Hall, 210 South 33rd St, Philadelphia, PA 19104, USA

[b]Department of Biomedical Engineering, University of Delaware, 125 East Delaware Avenue, Newark, DE 19716, USA

## Abstract

Despite the critical role tendons play in transmitting loads throughout the musculoskeletal system, little is known about the microstructural mechanisms underlying their mechanical function. Of particular interest is whether collagen fibrils in tendon fascicles bear load independently or if load is transferred between fibrils through interfibrillar shear forces. We conducted multiscale experimental testing and developed a microstructural shear lag model to explicitly test whether interfibrillar shear load transfer is indeed the fibrillar loading mechanism in tendon. Experimental correlations between fascicle macroscale mechanics and microscale interfibrillar sliding suggest that fibrils are discontinuous and share load. Moreover, for the first time, we demonstrate that a shear lag model can replicate the fascicle macroscale mechanics as well as predict the microscale fibrillar deformations. Since interfibrillar shear stress is the fundamental loading mechanism assumed in the model, this result provides strong evidence that load is transferred between fibrils in tendon and possibly other aligned collagenous tissues. Conclusively establishing this fibrillar loading mechanism and identifying the involved structural components should help develop repair strategies for tissue degeneration and guide the design of tissue engineered replacements.

### Keywords

Interfibrillar shear stress; Fibril sliding; Multiscale testing; Shear lag model; Tendon

## 1. Introduction

Tendons transfer muscle loads to the skeletal system and are thus essential for basic daily activity. However, the microstructural mechanisms underlying their mechanical function and their ability to bear load remain unknown. Tendon predominantly consists of type I collagen, which forms a complicated hierarchical organization spanning multiple lengths scales (Fig. 1) [1]. At the macroscopic level, tendons are separated into subunits called fascicles, which are dense collections of highly aligned collagen fibrils interspersed with cells [2,3]. While fibrils are recognized as the primary tensile load-bearing elements in tendon [4], it is



*Corresponding author. Tel.: +1 302 831 1295. delliott@udel.edu (D.M. Elliott).

unknown how the macroscopic loads applied to the fascicles are transmitted down to the individual fibrils. Identification of this fundamental fibrillar loading mechanism is necessary for determining the structural defects responsible for the loss of mechanical performance due to degeneration [5]. Ultimately, this information could be used to develop regenerative strategies to restore the tissue mechanical properties through cell-mediated remodeling, as well as guide the design of tissue engineered replacements.

A central unresolved question is whether collagen fibrils bear load independently or if the applied load is transferred across fibrils through interfibrillar shear forces. On the one hand, experimental observations of fibril branching and the lack of fibril ends in mature tissue suggest that loads are transmitted directly by continuous fibrils that span the full tissue length [6,7]. On the other hand, studies using X-ray diffraction and atomic force microscopy to measure fibril strains in tissues under tension have found that the fibril strains are less than half of the applied tissue strain [8–11]. These data imply that the collagen fibrils are discontinuous and that relative sliding between fibrils accounts for the difference between the tissue and fibril strains. If the fibrils are indeed discontinuous, then load must be transferred between fibrils, possibly via shear forces produced during their relative sliding. Indirect evidence for interfibrillar shear load transfer has been given by additional multiscale viscoelastic testing demonstrating that fibril strains are time dependent and behave similarly to the viscous response of the applied tissue stress but not the tissue strains [9,12–15]. These findings support the hypothesis of relative sliding between fibrils and also suggest that fibril loading is partly viscous in nature. Nevertheless, conclusions regarding the existence of interfibrillar shear load transfer are limited since these studies did not directly observe interfibrillar sliding and interpreted their findings with spring-dashpot mechanical models [8,12], which simplify the tissue structure into extensional elements and separate the model from the shear loading mechanisms being investigated.

The objective of this study is to explicitly test the hypothesis of interfibrillar shear load transfer in tendon by combining microscopic experimental techniques with a microstructural shear lag model. We used confocal microscopy to observe relative sliding between fibrils by measuring the microscale shear strains in tendon under uniaxial loading [12,16–20]. Additionally, the existence of load transfer between fibrils was explicitly tested with a shear lag model, which intrinsically defines interfibrillar shear as the fundamental fibrillar loading mechanism. While formulations of shear lag models have been applied to several biological tissues [21–33], this is the first time to our knowledge that a shear lag model has been applied to data obtained from multiscale tendon testing. Our results demonstrate that fascicle macroscale mechanics are strongly coupled to interfibrillar sliding. Furthermore, the shear lag model successfully reproduced the fascicle mechanics at both the macro- and microscopic length scales. These data suggest that interfibrillar shear load transfer is the physical mechanism underlying tendon fascicle macroscale mechanics.

## 2. Materials and methods

### 2.1. Multiscale experimental testing

Nine fascicles were harvested from the tails of three 8-month-old Sprague–Dawley rats that had been sacrificed for a separate IACUC-approved study. Rat tail fascicles are a widely

used tissue model for multiscale investigations of tendon [1,8,12,17–19]. Each fascicle was cut to a length of 45 mm and stained with an extracellular matrix fluorescent dye (5-DTAF, Invitrogen) [16]. Specifically, each sample was incubated for 20 min at room temperature in a 2 mg $ml^{-1}$ solution of 5-DTAF and 0.1 M sodium bicarbonate buffer (pH 9.0). This dye binds to the free amine groups of collagen molecules and has been used to visualize the microscale deformations of the extracellular matrix in several orthopaedic tissues [16,20,34–36]. The sample was washed in phosphate-buffered saline (PBS) and placed into the PBS bath of a uniaxial testing device mounted on an inverted confocal microscope (LSM 5 LIVE; 25X LD LCI Plan-Apochromat lens, Zeiss) (Fig. 2). A 1 mN preload (~8 kPa) was applied to the tissue to define the reference length (30.8 ± 0.1 mm). The sample was preconditioned by applying five cycles of 2% grip-to-grip strain at 1% $s^{-1}$, then allowed to recover at the reference length for 10 min. After the recovery period, a set of four lines (2.1 μm wide) separated by 100 μm were photobleached onto the tissue surface with a laser diode (489 nm, 100 mW) at three locations along the fascicle length: the sample center and ±5 mm from the center. In order to photobleach lines spanning the entire tissue width, line scans at maximum laser power were performed through the tissue depth in 5 μm increments. Microscale image stacks (15 fps; 0.53 × 0.53 × 1.24 μm $pixel^{-1}$) were taken of the initial positions of the photobleached lines and used to reconstruct the tissue cross-sectional profile, which was fitted with an ellipse to determine the sample cross-sectional area.

The testing protocol consisted of 2%, 4%, 6%, 8% and 10% applied grip strains, incrementally ramped at 1% $s^{-1}$, followed by a 30 min relaxation. While the stress relaxations at the 2% and 4% grip strains reached equilibrium, longer relaxation times were necessary for the larger applied strains (e.g., over 11 h for the 10% strain). However, 30 min was sufficient to reduce the rate of stress relaxation so that microscale measurements could be obtained at a quasi-static state (i.e. the load dropped by less than 2% during the 3 min image capture period). To measure the microscale deformations that occur during relaxation, image stacks of the photobleached lines were captured at the beginning and end of each relaxation period at the sample center (circles in Fig. 3). Due to the high frame rate of the imaging system, the image stacks were acquired over approximately 20 s and could be completed within the first 60 s of the relaxation period. At the other two locations, image stacks were taken only at the end of each relaxation period. The applied load was measured via a 10 N load cell (Model 31, Honeywell) and macroscale tissue strains were calculated by tracking the displacements of ink marks. Macroscale mechanical behavior was quantified by calculating the quasi-static tensile modulus and incremental percent relaxation at each applied strain value (Fig. 3).

### 2.2. Data analysis

After testing, the microscale image stacks were converted to a single composite image of the full tissue width. Due to the curved tissue surface, each individual image taken at a particular focal plane contains narrow vertical bands of signal intensity (Fig. 4). To form a single image composite, the images containing signal intensity at a particular *x*-position were determined. The intensity values in the vertical line of pixels at this *x*-position were then averaged across the selected images. The composite image of the full tissue width was produced by repeating this process for each *x*-position and concatenating the averaged

vertical lines. A custom Matlab algorithm was used to find the pixel locations of the four photobleached lines. Briefly, at a given position along the *x*-direction, the *y*-position of each line was determined by the pixel with the minimum intensity in the composite image. These values were smoothed by computing a moving average across each line with an averaging window of 35 pixels.

At each *x*-position and between each pair of lines, fibril strains ($\varepsilon_y$) were calculated as the change in the distance between line pairs compared to their positions at 0% applied strain (Fig. 5A). Microscale shear strains ($\gamma$) were measured as the angle made between each line and the direction perpendicular to the fascicle axis. The overall level of interfibrillar sliding was quantified by the tortuosity (i.e. waviness) of the photobleached lines, which can be represented by the spread of the measured shear strains. This was calculated by averaging the angles across the four photobleached lines to obtain a single distribution of shear strains across the sample width, then computing the standard deviation of this average angular profile (Fig. 5D). For the fibril strains, a representative fibril:tissue strain ratio was calculated as the average fibril strain divided by the macroscale tissue strain. The fibril:tissue strain ratio and interfibrillar sliding averaged across the three microscale imaging locations were used for parametric statistical analyses (see Section 2.4).

## 2.3. Shear lag model

**2.3.1. Model formulation—**Shear lag models are commonly used to represent composite materials composed of discontinuous stiff fibers embedded in a soft matrix. The fundamental assumption of these models is that the externally applied load is transferred to the fibers through shear stresses acting at the fiber–matrix interface. Therefore, a microstructural shear lag model was used to explicitly test whether shear load transfer between discontinuous sliding fibrils is an accurate representation of the physical mechanisms underlying tendon fascicle mechanics. The fascicle structure was simplified as a periodic array of discontinuous and staggered fibrils (Fig. 6) [21,29]. Individual collagen fibrils exhibit non-linear strain stiffening behavior [37]. This was approximated by assuming that the fibrils are initially crimped and bear load only after being uncrimped. Since fibrils are not uniformly crimped within a fascicle [1,38], a gamma probability distribution was used to represent the spread of tissue stretches required to uncrimp the unit cell of fibrils [39,40]. Note that, once uncrimped, each unit cell is half the length of the uncrimped fibril length (*L*).

At any point *x* where there is relative sliding between the uncrimped fibrils, an interfibrillar shear stress ($\tau(x)$) acts equally over the entire fibril circumference (Fig. 6B), leading to the following equilibrium equation:

$$\frac{d\sigma_1(x)}{dx}=\frac{2\tau(x)}{r}=-\frac{d\sigma_2(x)}{dx} \quad (1)$$

where $\sigma_i(x)$ is the stress in the *i*th fibril and *r* is the fibril radius. Note that the ends of the fibrils are unloaded and *P* is the stress at the fibril midpoint. Based on the results of our multiscale experimental testing (see Discussion), we chose to use a perfectly plastic

constitutive relationship for the interfibrillar shear stress (i.e. interfibrillar sliding produces a constant interfibrillar shear stress):

$$\tau(x)=\tau \quad \text{for} \quad u_1(x) \neq u_2(x) \quad (2)$$

$$\tau(x)=0 \quad \text{for} \quad u_1(x)=u_2(x) \quad (3)$$

where $u_i(x)$ is the displacement of the *i*th fibril. It was also assumed that, once uncrimped, the fibrils were linear elastic and that the axial displacements of the fibrils are uniform throughout their cross-section (no intrafibrillar shear). By enforcing compatibility along the fibril length and using the boundary condition $u_1(L/2) = -u_2(0) = U/2$, direct integration leads to the following piecewise solutions for the fibril stress and displacement (Fig. 6C and E):

$$\sigma_1(x)=\begin{cases} 2\tau x/r & 0 \le x \le L_S \\ 2\tau L_S/r=P/2 & L_S \le x \le L/2-L_S \\ 2\tau(x-L/2+2L_S)/r & L/2-L_S \le x \le L/2 \end{cases} \quad (4)$$

$$u_1(x)=\begin{cases} \tau(x^2+L_S^2-L_SL/2)/rE & 0 \le x \le L_S \\ \tau L_S(2x-L/2)/rE & L_S \le x \le L/2-L_S \\ \tau[x^2+L_S^2+(L/2)^2+(4L_S-L)x-3L_SL/2]/rE & L/2-L_S \le x \le L/2 \end{cases} \quad (5)$$

$$L_S=-L/4+\sqrt{(L/4)^2+(rEL/4\tau)\varepsilon_{uc}} \quad (6)$$

where $L$ and $E$ are the fibril length and modulus, respectively, and $L_S$ is the length from the fibril ends over which there is relative sliding between fibrils. The strain of the uncrimped unit cell ($\varepsilon_{uc}$) is given by

$$\varepsilon_{uc}=2U/L=\lambda/\lambda_c-1 \quad (7)$$

where $\lambda$ is the applied tissue stretch and $\lambda_c$ is the tissue stretch required to uncrimp this unit cell. Note that the stress averaged over the two fibrils at any point $x$ along the unit cell is $P/2$ (Fig. 6C). Therefore, the average stress in the uncrimped unit cell is

$$\sigma_{uc}=P/2=\tau/r\left[\sqrt{L^2/4+(rEL/\tau)\varepsilon_{uc}}-L/2\right] \quad (8)$$

Finally, homogenization to calculate the macroscale tissue stress ($\sigma_T$) is performed by integrating $\sigma_{uc}$ across the possible uncrimping stretches weighted by the probability that a unit cell has a given uncrimping stretch ($g(\lambda_c - 1)$) and then multiplying by the fibril volume fraction ($\phi$)

$$\sigma_T(\lambda)=\phi\int_0^{\lambda}\sigma_{uc}g(\lambda_c-1)d\lambda_c. \quad (9)$$

While our model shares the same governing equation (Eq. (1)) as elastic shear lag models [21,41], the assumption of plasticity at the fibril–matrix interface has an important consequence. In elastic models, interfibrillar sliding occurs over a fixed distance from the fibril ends, independent of the load or strain applied to the tissue. However, in the case of a constant interfibrillar shear stress, the length over which load is transferred between fibrils increases with greater applied strain (Eq. (6)) since the only way to increase the load applied to the fibrils is to increase the surface area over which the interfibrillar shear stress acts. Ultimately, sliding will occur over the entire length of the fibrils ($L_S = L/4$) and the interfibrillar shear stress will act on the complete fibril surface area, at which point $\sigma_{uc}$ reaches a maximum value of $\tau L/2r$ (Fig. 6F–H). Any tissue strain beyond this level will simply cause the fibrils to slide without further elongation.

**2.3.2. Model fit of macroscale mechanics—**This model formulation contains seven parameters: interfibrillar shear stress ($\tau$), fibril volume fraction ($\phi$), fibril radius ($r$), fibril length ($L$), fibril modulus ($E$), the mean uncrimping stretch ($\overline{\lambda}_c$) and the standard deviation of uncrimping ($\lambda_c^{SD}$). Based on existing data, the fibril radius and volume fraction were assumed as 85 nm and 0.7, respectively [42,43]. Previous measurements of fibril lengths in fetal tendon [44] and the tissue reference length were used as guidelines for choosing 1 and 25 mm as the bounds for fibril length. The remaining four parameters ($\tau$, $E$, $\overline{\lambda}_c$, $\lambda_c^{SD}$) were determined by fitting Eq. (9) to the experimentally measured quasi-static macroscale tissue response using a trust-region-reflective least-squares algorithm (Matlab). To check the accuracy of the uncrimping parameters, the 95th-percentile uncrimping stretch (i.e. mean plus two standard deviations) determined from the gamma cumulative distribution function was compared to the applied tissue stretch at which the crimp waveform was no longer visible in the macroscale images [17].

**2.3.3. Model prediction of microscale deformations—**After determining the model parameters from the macroscale data, the model was used to predict the fibril:tissue strain ratio as a function of the applied tissue strain. Since these data were not used for calculating the model parameters, this microscale prediction explicitly tests whether the physical mechanisms embedded in the model accurately represent the true loading mechanisms in tendon fascicles. It is important to note that the fibril strains observed with the microscope include the tissue stretch required to uncrimp the fibrils. That is, the experimentally observed (apparent) fibril strains are not simply the strains for which the fibrils bear load, but are the cumulative elongation of the fibrils normalized by their original crimped length. Therefore, the equivalent apparent strain ($\varepsilon_{app}$) of the uncrimped fibrils predicted by the model is

$$\varepsilon_{app} = (1 + \sigma_{uc}/E)\lambda_c - 1 \quad (10)$$

Prior to uncrimping, the apparent fibril strain is equal to the tissue strain. Again using a gamma distribution for uncrimping stretches, the apparent fibril:tissue strain ratio ($\eta$) predicted by the model is

$$\eta(\lambda)=[1-G(\lambda-1)]+(\lambda-1)^{-1}\int_0^{\lambda}\varepsilon_{\mathrm{app}}g(\lambda_c-1)d\lambda_c \quad (11)$$

where $G(\lambda - 1)$ is the gamma cumulative distribution function. Note that the first term represents the fibrils that are still crimped and, therefore, have the same apparent strain as the tissue. To validate the model, values of Eq. (11) calculated at each applied tissue strain were compared with the experimental fibril:tissue strain ratio averaged across the three microscale imaging locations.

### 2.4. Statistical analysis

The consistency of the interfibrillar sliding and fibril:tissue strain ratio measurements along the fascicle length was determined by the coefficient of variation calculated across the three microscale imaging locations. The level of interfibrillar sliding was correlated with the fibril:tissue strain ratio, the macroscale quasi-static modulus and the percent stress relaxation to determine if these mechanical properties are related to interfibrillar sliding. To evaluate whether time-dependent microscale deformations are related to the macroscale stress relaxation, the percent change in the interfibrillar sliding and fibril:tissue strain ratio during the relaxation periods were correlated with the drop in stress between the microscale imaging time points. Parametric tests were used for all statistical analyses, with significance set at $p < 0.05$, and data are presented as mean ± standard deviation.

## 3. Results

### 3.1. Multiscale experimental testing

The displacements of photobleached lines observed under a confocal microscope were used to measure the interfibrillar sliding, and the ratio between fibril and tissue strains in rat tail fascicles in uniaxial tension. The values obtained for both the interfibrillar sliding and fibril:tissue strain ratio were consistent across the three imaging locations, with average coefficients of variation of 0.16 ± 0.07 and 0.057 ± 0.046, respectively (Fig. 7). This demonstrates that the measurements represent the microscale deformations throughout the tissue and, therefore, can be used to accurately quantify the relationship between interfibrillar sliding and macroscale fascicle mechanics.

At the macroscopic length scale, increasing tissue strains led to a decrease in the quasi-static modulus ($r = -0.97$, $p < 0.01$) and an increase in the stress relaxation ($r = 0.99$, $p < 0.001$) (Fig. 8A and B). This strain-softening behavior prior to complete rupture is typical for fascicles strained beyond their elastic limit [33]. The microscale deformations exhibited patterns similar to the macroscale behavior, with the fibril:tissue strain ratio decreasing ($r = -0.99$, $p < 0.001$) and the interfibrillar sliding increasing ($r = 0.99$, $p < 0.001$) with applied tissue strain (Fig. 8C and D). The concomitant decrease in fibril strains and increase in interfibrillar sliding support the hypothesis that fibrils are discontinuous and that the macroscale tissue strain results from the combination of fibril elongation and sliding. Furthermore, we would expect that more interfibrillar sliding would reduce the macroscale tissue stiffness since less strain is being transmitted directly to the fibrils. Linear correlations with the level of interfibrillar sliding confirmed this hypothesis, demonstrating that the fibril:tissue strain ratio ($r = -0.92$, $p < 0.0001$) and the macroscale quasi-static modulus ($r =$

−0.81, $p < 0.0001$) both decrease with greater interfibrillar sliding (Fig. 9A and B). Collectively, these data suggest that increased interfibrillar sliding is responsible for the drop in tissue modulus observed in the post-yield tensile behavior of tendon fascicles.

The multiscale experimental data was also used to investigate the constitutive nature of the interfibrillar shear load transfer that would necessarily exist in tendon fascicles composed of discontinuous fibrils. Similarities between the fibril strains and the tissue stress during previous multiscale viscoelastic testing provided indirect evidence that a viscous interfibrillar shear load transfer is associated with interfibrillar sliding [9,12–15]. Our current findings that interfibrillar sliding is strongly correlated with increased macroscale stress relaxation ($r = 0.94$, $p < 0.0001$) directly supports this hypothesis (Fig. 9C). Furthermore, we measured the changes in the microscale deformations that occurred during the relaxation periods to determine whether an interfibrillar shear load transfer is responsible for the macroscale stress relaxation. On average, the fibril strains decreased (−7.4 ± 4.1%, $p < 0.0001$) and the interfibrillar sliding increased (10.7 ± 8.0%, $p < 0.0001$) during the relaxation periods. This behavior not only ensures compatibility with the fixed macroscale boundary conditions but also demonstrates that interfibrillar sliding is time dependent and is related to the stress relaxation in the tissue. Additionally, the drop in fibril strain during the relaxation periods was significantly correlated with the amount of stress relaxation ($r = 0.80$, $p < 0.0001$). This finding suggests that interfibrillar sliding contributes to the macroscale stress relaxation by slowly unloading the fibrils over time. Together, these observations support the existence of a viscous interfibrillar shear stress that resists interfibrillar sliding and transmits load between fibrils.

### 3.2. Shear lag model

A microstructural shear lag model composed of crimped discontinuous fibrils was developed to explicitly test whether interfibrillar shear load transfer can explain the observed multiscale fascicle mechanics. The four model parameters – interfibrillar shear stress ($\tau$), fibril modulus ($E$), mean uncrimping stretch ($\overline{\lambda}_c$) and standard deviation of uncrimping ($\lambda_c^{SD}$) – were determined by fitting the model to the quasi-static macroscale tissue mechanics. The model fits of the macroscale behavior were excellent (Fig. 10A; $R^2 = 0.996 \pm 0.003$). The fibril model parameters were independent of the choice for fibril length and had the following values: $E = 1.6 \pm 0.4$ GPa, $\overline{\lambda}_c = 1.002 \pm 0.0008$ and $\lambda_c^{SD} = 0.001 \pm 0.0007$. While the fibril modulus is relatively high compared to previous findings [37,45–47], it is within a factor of two of the maximum fascicle quasi-static modulus. This is comparable to the factor of 1.4 that would be expected for the ratio of the fibril-to-tissue moduli for a composite tissue composed of continuous fibrils with the same fibril volume fraction. The uncrimping parameters accurately described the tissue crimp, since the 95th-percentile uncrimping stretch predicted by the model (1.004 ± 0.002) was not significantly different from the experimental tissue stretch at which the crimp pattern was seen to disappear (1.004 ± 0.001). The interfibrillar shear stress was inversely proportional to fibril length ($L$), with values of 8.6 ± 2.7 kPa for $L = 1$ mm and 0.35 ± 0.11 kPa for $L = 25$ mm, which are similar to values obtained from macroscale shear tests of ligament [48]. The success of the model in accurately representing the loading mechanism in tendon fascicles is best demonstrated by the very good prediction of the experimental fibril:tissue strain ratio (Fig. 10B; $R^2 = 0.74 \pm$

0.18). Since these data were not used to calculate the model parameters, the successful prediction of the microscale deformations validates the physical mechanisms embedded in the model and suggests that load is indeed transferred between discontinuous fibrils through interfibrillar shear stresses.

## 4. Discussion

This study strongly suggests that collagen fibrils in tendon are indeed loaded via interfibrillar shear produced by the relative sliding of fibrils. Simultaneous measurement of fascicle macroscale mechanics and microscale deformations clearly indicated that the tissue mechanics is correlated to the amount of interfibrillar sliding. Increased sliding reduced the amount of strain that is transmitted to the fibrils, and therefore lowered the tissue macroscale modulus (Fig. 9A and B). This is consistent with the hypothesis that collagen fibrils are discontinuous and transmit load via interfibrillar shear. Furthermore, the data agree with previous suggestions that interfibrillar shear stresses are viscous in nature [9,12–15]. Interfibrillar sliding was observed to increase during the stress relaxation periods, which likely contributed to the time-dependent drop in fibril strains and tissue stress. This allows the tissue to dissipate energy via the relative sliding between fibrils, as seen by the correlation between interfibrillar sliding and stress relaxation (Fig. 9C). However, the clearest demonstration of interfibrillar shear load transfer in tendon is given by the ability of a shear lag model to successful replicate the multiscale fascicle mechanics. The macroscale behavior was fitted exceptionally well (Fig. 10A), and produced model parameters that are physically reasonable and agree with existing data [48]. More importantly, the model was able to successfully predict the fibril strains (Fig. 10B), which was an independent data set not used for determination of the model parameters. This validation of the model across both length scales is strong evidence that interfibrillar shear load transfer between discontinuous fibrils, which was explicitly assumed in the model construction, is indeed the fibril loading mechanism in tendon fascicles.

It should be noted that the fibril:tissue strain ratio measured in the current study is substantially higher than values found previously [8,16–18]. In contrast to X-ray diffraction, microscale deformations measured using confocal microscopy include both fibril strains that mechanically load the fibrils and strains that occur with uncrimping. While this produces apparent fibril strains that are larger than the strains due to actual fibril loading, this effect was accounted for when making comparisons with the model microscale predictions (see Section 2.3.3). Additionally, confocal microscopy lacks the resolution to observe individual fibrils and, therefore, to directly measure fibril strains and interfibrillar sliding. However, the continuity of the photobleached lines seen here (Fig. 5) and by other investigators [19] confirms that the shear deformations observed under the microscope occur between the fibrils themselves and not just at the interface of fibril bundles (i.e. fibers). Furthermore, each pixel in the microscale images is only about three times the width of the average fibril diameter [42]; therefore, the strains calculated from the photobleached line displacements are a local homogenization of the individual fibril strains. This demonstrates that the use of confocal microscopy allows for representative measurements of local fibril deformations.

Several technical advantages also may explain the differences between our results and those from other confocal microscopy studies. Previous studies used grip-to-grip strains to calculate the fibril:tissue strain ratio [16–19], whereas we measured the actual tissue strains by optically tracking the displacements of ink markers. On average, we found that the tissue strains were 80% of the applied grip-to-grip strains, which is common for tensile testing of tendon fascicles [49]. Hence, use of grip-to-grip strains will underestimate the fibril:tissue strain ratio. Additionally, we directly measured the microscale displacements of the extracellular matrix using photobleached lines. Some previous studies instead made indirect measurements by tracking the displacements of cell nuclei [17,18], which produce lower microscale strain values than photobleached lines [19]. Finally, it is possible that earlier microscale measurements were not representative of the deformations across the entire tissue. Previous confocal experiments only imaged a single focal plane and, due to the elliptical fascicle shape, measured microscale deformations over a small portion of the sample width (Fig. 4) [16]. By capturing microscale image stacks through the full tissue depth, we obtained measurements across the entire fascicle width. Comparing microscale measurements made at multiple locations within each sample, we found that our measurements are consistent across the sample length (Fig. 7) and are likely representative of the deformations throughout the tissue.

While this study indicates that shear load transfer exists between discontinuous fibrils, it is still unclear what tissue components serve to transmit interfibrillar shear forces. The glycosaminoglycan (GAG) chains of the small leucine-rich proteoglycans found in tendons have been traditionally suggested as possible interfibrillar mechanical linkages [25,29,50,51]. However, several experimental studies that selectively removed GAGs via enzymatic digestions failed to demonstrate any effect on tendon or ligament macroscale mechanics [52–55]. Although computational models demonstrate that these findings may still be consistent with the hypothesis that GAGs transmit load between fibrils [21], these models assume covalent linkages between GAG chains [29,30], which may overestimate the stiffness of their interactions [56]. Furthermore, ultrastructural investigations have found that fibril strains are higher in tendons without GAGs, suggesting that GAGs may serve to actually reduce load transmission between fibrils [57]. Other possibilities include the FACIT family of molecules, specifically collagen types XIV and XII. While they are involved in fibrillogenesis, their relative absence in mature tissues and minimal effect on tendon mechanics do not support a role in interfibrillar load transfer [58,59]. Nevertheless, the mechanical contribution of myriad other tissue components (e.g. collagens XX, XXI, emu1/emu2, COMP) are yet to be determined [50,60].

The most important consideration in using a shear lag model is the choice of the constitutive relationship between the shear strain and stress of the interfibrillar matrix. Elastic relationships (e.g. constant shear modulus) can replicate the linear portion of the macroscale response; however, they predict a tissue modulus and fibril:tissue strain ratio that are independent of the applied tissue strain [41], which does not agree with our experimental data (Fig. 8A and C). While these data can be reproduced by progressive fibril rupture causing a reduction in fibril lengths, structural investigations do not support this possibility. Tendon fascicles stretched beyond their yield point contain fibrils with localized plastic deformation that do not show signs of rupture until after a substantial amount of fatigue

loading (>20,000 cycles) [61,62]. Yielding of the collagen fibrils can explain the strain softening observed in the macroscale mechanics (Fig. 8A); however, a reduction in the fibril modulus would increase the fibril strains and produce an increase in the fibril:tissue strain ratio, which contradicts our microscale data (Fig. 8C). In contrast to these other hypotheses, plastic behavior at the fibril–matrix interface can reproduce the full multiscale dataset. The assumption of a constant interfibrillar shear stress is the simplest representation of interfibrillar plasticity [24–28,63]. We avoided using more complicated formulations that are based on the failure of specific components of the interfibrillar matrix because of the current controversy regarding the structural elements involved in load transfer between fibrils. Nevertheless, our model successfully replicated the entire quasi-static macroscale stress–strain curve and accurately predicted the fibril:tissue strain ratios. This suggests not only that interfibrillar shear is responsible for loading the collagen fibrils, but that plasticity at the fibril–matrix interface may contribute to the subfailure behavior of tendon fascicles.

Although our model assumes that the fibril–matrix interface is purely plastic, it is likely that the interfibrillar shear response is initially elastic and that other processes, like fibril yielding, are also involved at higher applied tissue strains. The D-period spacing of fibrils becomes disrupted at high strains before tissue failure [11,14,46,61,64–67]. This behavior suggests that sliding occurs between collagen molecules within the fibrils, which may cause the fibrils to yield [31,32]. Including the effects of fibril yielding by adding these deformations at the sub-fibril hierarchical level to the current model may improve the model's prediction of the experimental data. Regarding the exclusion of any initial elasticity for interfibrillar sliding, given the low plastic shear stress value estimated by our model (~1 kPa), the initial elastic behavior at stresses below this magnitude is likely insignificant. Additionally, a purely plastic response of the interfibrillar matrix can still produce elastic behavior at the macroscopic level; the elasticity of the fibrils is sufficient to bring the tissue back to its preconditioned state upon removal of the applied load [24]. Finally, while a perfectly plastic constitutive response is likely a simplification of the mechanics at the fibril–matrix interface, using a constant stress value provides an order-of-magnitude estimate that can offer insight into which structural components are involved in transmitting loads between fibrils and, therefore, which alternative constitutive behaviors are possible.

A limitation of the current model is that only the quasi-static tissue behavior was fitted by the model and all time-dependent effects were ignored. Previous studies have suggested that the interfibrillar shear stress is dependent on both strain rate and time [8,9,12–15]. Our finding that fibril unloading is correlated with the magnitude of stress relaxation supports this hypothesis. Shear thickening of the interfibrillar matrix (i.e. increased shear stress with strain rate) can also explain the stiff response of the tissue during the last 1% $s^{-1}$ strain ramp despite the plateau in the quasi-static behavior (Fig. 10A). Furthermore, a viscoplastic interfibrillar shear stress is consistent with the creep failure of tendons held at stresses significantly below their ultimate tensile strength [68]. However, several other phenomena, including poroelastic effects and the intrinsic viscoelasticity of collagen fibrils, may also contribute to the macroscale time-dependent behavior [37,69–71]. For the current study we chose to disregard time-dependent effects in order to focus on the objective of evaluating the specific role of interfibrillar shear load transfer on fascicle mechanics. In the future, it would be useful to develop a model that combines these other time-dependent phenomena with a

viscoplastic interfibrillar shear stress to determine their contributions to the full time-dependent behavior of tendons.

In conclusion, our multiscale experimental testing and mechanical modeling suggest that interfibrillar shear load transfer between discontinuous fibrils is the mechanism underlying tendon fascicle mechanics. These findings have important implications for tissue failure and treatment. The nonlinear elastic response of collagenous tissues under uniaxial tension has previously been explained by the straightening and reorientation of crimped fibrils into the direction of applied load, as well as the deformations of the fibrils themselves [4,11]. Our current results extend this knowledge beyond the elastic limit, suggesting that interfibrillar sliding is not only involved in the elastic tissue behavior but also produces the post-yield drop in tissue stiffness. Identifying the mechanisms that reduce the tissue's ability to bear load is required to understand how degeneration affects tissue mechanics and ultimately leads to complete rupture. Additionally, for the first time to our knowledge, we have demonstrated that a shear lag model, based on shear load transfer between discontinuous fibrils, can not only approximate the macroscale tissue mechanics through the full stress–strain curve, but can also predict the microscale deformations. Discovering the relationship between tissue hierarchical structure and mechanical behavior is a prerequisite for engineering functional tissue replacements that can recapitulate normal mechanical function. Finally, while this work focused on the multiscale mechanics of tendon fascicles, it is likely that these conclusions regarding interfibrillar shear load transfer extend more broadly to other aligned collagenous tissues as well.

## Acknowledgments

This research was supported by an NIH COBRE Grant (NIH/NCRR P20 RR016458). We thank Dr. Jeffrey Caplan, Director of the Bioimaging Center, at the Delaware Biotechnology Institute for his valuable assistance in using the confocal microscope for our testing. We are also grateful to Prof. Louis J. Soslowsky for providing the rat tails used for our experiments.

## Appendix A. Figures with essential colour discrimination

Certain figures in this article, particularly Fig. 5, is difficult to interpret in black and white. The full colour images can be found in the on-line version, at http://dx.doi.org/10.1016/j.actbio.2014.01.032.

## References

1. Kastelic J, Galeski A, Baer E. The multicomposite structure of tendon. Connect Tissue Res. 1978; 6:11–23. [PubMed: 149646]
2. Rowe RW. The structure of rat tail tendon. Connect Tissue Res. 1985; 14:9–20. [PubMed: 2934217]
3. Torp, S.; Baer, E.; Friedman, B. Effects of age and of mechanical deformation on the ultrastructure of tendon. In: Atkins, ED.; Keller, A., editors. Structure of fibrous biopolymers. London: Colston Research Society; 1975. p. 223-50.
4. Lanir Y. Constitutive equations for fibrous connective tissues. J Biomech. 1983; 16:1–12. [PubMed: 6833305]
5. Cook JL, Purdam CR. Is tendon pathology a continuum? A pathology model to explain the clinical presentation of load-induced tendinopathy. Br J Sports Med. 2009; 43:409–16. [PubMed: 18812414]

6. Provenzano PP, Vanderby R Jr. Collagen fibril morphology and organization: implications for force transmission in ligament and tendon. Matrix Biol. 2006; 25:71–84. [PubMed: 16271455]
7. Starborg T, Lu Y, Huffman A, Holmes DF, Kadler KE. Electron microscope 3D reconstruction of branched collagen fibrils in vivo. Scand J Med Sci Sports. 2009; 19:547–52. [PubMed: 19422644]
8. Puxkandl R, Zizak I, Paris O, Keckes J, Tesch W, Bernstorff S, et al. Viscoelastic properties of collagen: synchrotron radiation investigations and structural model. Philos Trans R Soc Lond B Biol Sci. 2002; 357:191–7. [PubMed: 11911776]
9. Liao J, Yang L, Grashow J, Sacks MS. The relation between collagen fibril kinematics and mechanical properties in the mitral valve anterior leaflet. J Biomech Eng. 2007; 129:78–87. [PubMed: 17227101]
10. Rigozzi S, Stemmer A, Müller R, Snedeker JG. Mechanical response of individual collagen fibrils in loaded tendon as measured by atomic force microscopy. J Struct Biol. 2011; 176:9–15. [PubMed: 21771659]
11. Fratzl P, Misof K, Zizak I, Rapp G, Amenitsch H, Bernstorff S. Fibrillar structure and mechanical properties of collagen. J Struct Biol. 1998; 122:119–22. [PubMed: 9724612]
12. Gupta HS, Seto J, Krauss S, Boesecke P, Screen HRC. In situ multi-level analysis of viscoelastic deformation mechanisms in tendon collagen. J Struct Biol. 2010; 169:183–91. [PubMed: 19822213]
13. Nemetschek T, Jelinek K, Knörzer E, Mosler E, Nemetschek-Gansler H, Riedl H, et al. Transformation of the structure of collagen. A time-resolved analysis of mechanochemical processes using synchrotron radiation. J Mol Biol. 1983; 167:461–79. [PubMed: 6864805]
14. Mosler E, Folkhard W, Knörzer E, Nemetschek-Gansler H, Nemetschek T, Koch MH. Stress-induced molecular rearrangement in tendon collagen. J Mol Biol. 1985; 182:589–96. [PubMed: 4009715]
15. Sasaki N, Shukunami N, Matsushima N, Izumi Y. Time-resolved X-ray diffraction from tendon collagen during creep using synchrotron radiation. J Biomech. 1999; 32:285–92. [PubMed: 10093028]
16. Cheng V, Screen H. The micro-structural strain response of tendon. J Mater Sci. 2007; 42:8957–65.
17. Screen HRC, Lee DA, Bader DL, Shelton JC. An investigation into the effects of the hierarchical structure of tendon fascicles on micromechanical properties. Proc Inst Mech Eng [H]. 2004; 218:109–19.
18. Li Y, Fessel G, Georgiadis M, Snedeker JG. Advanced glycation end-products diminish tendon collagen fiber sliding. Matrix Biol. 2013; 32:169–77. [PubMed: 23348249]
19. Duncan NA, Bruehlmann SB, Hunter CJ, Shao X, Kelly EJ. In situ cell–matrix mechanics in tendon fascicles and seeded collagen gels: implications for the multiscale design of biomaterials. Comput Methods Biomech Biomed Engin. 2014; 17:39–47. [PubMed: 23237459]
20. Bruehlmann SB, Matyas JR, Duncan NA. ISSLS prize winner: collagen fibril sliding governs cell mechanics in the anulus fibrosus: an in situ confocal microscopy study of bovine discs. Spine. 2004; 29:2612–20. [PubMed: 15564909]
21. Ahmadzadeh H, Connizzo BK, Freedman BR, Soslowsky LJ, Shenoy VB. Determining the contribution of glycosaminoglycans to tendon mechanical properties with a modified shear-lag model. J Biomech. 2013; 46:2497–503. [PubMed: 23932185]
22. Jäger I, Fratzl P. Mineralized collagen fibrils: a mechanical model with a staggered arrangement of mineral particles. Biophys J. 2000; 79:1737–46. [PubMed: 11023882]
23. Gao H, Ji B, Jäger IL, Arzt E, Fratzl P. Materials become insensitive to flaws at nanoscale: lessons from nature. Proc Natl Acad Sci USA. 2003; 100:5597–600. [PubMed: 12732735]
24. Mijailovich SM, Stamenović D, Fredberg JJ. Toward a kinetic theory of connective tissue micromechanics. J Appl Physiol. 1993; 74:665–81. [PubMed: 8458781]
25. Ciarletta P, Ben Amar M. A finite dissipative theory of temporary interfibrillar bridges in the extracellular matrix of ligaments and tendons. J R Soc Interface. 2009; 6:909–24. [PubMed: 19106068]

26. Goh KL, Meakin JR, Aspden RM, Hukins DWL. Stress transfer in collagen fibrils reinforcing connective tissues: effects of collagen fibril slenderness and relative stiffness. J Theor Biol. 2007; 245:305–11. [PubMed: 17123548]
27. Gao Y, Wineman AS, Waas AM. Mechanics of muscle injury induced by lengthening contraction. Ann Biomed Eng. 2008; 36:1615–23. [PubMed: 18686034]
28. Aspden RM. Fibre reinforcing by collagen in cartilage and soft connective tissues. Proc Biol Sci. 1994; 258:195–200. [PubMed: 7838856]
29. Redaelli A, Vesentini S, Soncini M, Vena P, Mantero S, Montevecchi FM. Possible role of decorin glycosaminoglycans in fibril to fibril force transfer in relative mature tendons – a computational study from molecular to microstructural level. J Biomech. 2003; 36:1555–69. [PubMed: 14499303]
30. Fessel G, Snedeker JG. Equivalent stiffness after glycosaminoglycan depletion in tendon – an ultra-structural finite element model and corresponding experiments. J Theor Biol. 2011; 268:77–83. [PubMed: 20950629]
31. Buehler MJ. Nature designs tough collagen: explaining the nanostructure of collagen fibrils. Proc Natl Acad Sci USA. 2006; 103:12285–90. [PubMed: 16895989]
32. Tang Y, Ballarini R, Buehler MJ, Eppell SJ. Deformation micromechanisms of collagen fibrils under uniaxial tension. J R Soc Interface. 2010; 7:839–50. [PubMed: 19897533]
33. Torp, S.; Arridge, RG.; Armeniades, CD.; Baer, E. Structure–property relationships in tendon as a function of age. In: Atkins, ED.; Keller, A., editors. Structure of fibrous biopolymers. London: Colston Research Society; 1975. p. 197-221.
34. Upton ML, Gilchrist CL, Guilak F, Setton LA. Transfer of macroscale tissue strain to microscale cell regions in the deformed meniscus. Biophys J. 2008; 95:2116–24. [PubMed: 18487290]
35. Michalek AJ, Buckley MR, Bonassar LJ, Cohen I, Iatridis JC. Measurement of local strains in intervertebral disc annulus fibrosus tissue under dynamic shear: contributions of matrix fiber orientation and elastin content. J Biomech. 2009; 42:2279–85. [PubMed: 19664773]
36. Buckley MR, Bergou AJ, Fouchard J, Bonassar LJ, Cohen I. High-resolution spatial mapping of shear properties in cartilage. J Biomech. 2010; 43:796–800. [PubMed: 19896130]
37. Yang L, van der Werf KO, Dijkstra PJ, Feijen J, Bennink ML. Micromechanical analysis of native and cross-linked collagen type I fibrils supports the existence of microfibrils. J Mech Behav Biomed Mater. 2012; 6:148–58. [PubMed: 22301184]
38. Rowe RW. The structure of rat tail tendon fascicles. Connect Tissue Res. 1985; 14:21–30. [PubMed: 2934212]
39. Szczesny SE, Peloquin JM, Cortes DH, Kadlowec JA, Soslowsky LJ, Elliott DM. Biaxial tensile testing and constitutive modeling of human supraspinatus tendon. J Biomech Eng. 2012; 134:021004. [PubMed: 22482671]
40. Sacks MS. Incorporation of experimentally-derived fiber orientation into a structural constitutive model for planar collagenous tissues. J Biomech Eng. 2003; 125:280–7. [PubMed: 12751291]
41. Hull, D.; Clyne, TW. An introduction to composite materials. Cambridge: Cambridge University Press; 1996.
42. Parry, DA.; Craig, AS. Growth and development of collagen fibrils in connective tissue. In: Ruggeri, A.; Motta, PM., editors. Ultrastructure of the connective tissue matrix. Boston, MA: Martinus Nijhoff; 1984. p. 34-64.
43. Screen HRC, Shelton JC, Chhaya VH, Kayser MV, Bader DL, Lee DA. The influence of noncollagenous matrix components on the micromechanical environment of tendon fascicles. Ann Biomed Eng. 2005; 33:1090–9. [PubMed: 16133917]
44. Birk DE, Nurminskaya MV, Zycband EI. Collagen fibrillogenesis in situ: fibril segments undergo post-depositional modifications resulting in linear and lateral growth during matrix development. Dev Dyn. 1995; 202:229–43. [PubMed: 7780173]
45. Van der Rijt JAJ, van der Werf KO, Bennink ML, Dijkstra PJ, Feijen J. Micromechanical testing of individual collagen fibrils. Macromol Biosci. 2006; 6:697–702. [PubMed: 16967482]
46. Sasaki N, Odajima S. Elongation mechanism of collagen fibrils and force–strain relations of tendon at each level of structural hierarchy. J Biomech. 1996; 29:1131–6. [PubMed: 8872269]

47. Gautieri A, Vesentini S, Redaelli A, Buehler MJ. Hierarchical structure and nanomechanics of collagen microfibrils from the atomistic scale up. Nano Lett. 2011; 11:757–66. [PubMed: 21207932]
48. Bonifasi-Lista C, Lake SP, Small MS, Weiss JA. Viscoelastic properties of the human medial collateral ligament under longitudinal, transverse and shear loading. J Orthop Res. 2005; 23:67–76. [PubMed: 15607877]
49. Haraldsson BT, Aagaard P, Krogsgaard M, Alkjaer T, Kjaer M, Magnusson SP. Region-specific mechanical properties of the human patella tendon. J Appl Physiol. 2005; 98:1006–12. [PubMed: 15448120]
50. Thorpe CT, Birch HL, Clegg PD, Screen HRC. The role of the non-collagenous matrix in tendon function. Int J Exp Pathol. 2013; 94:248–59. [PubMed: 23718692]
51. Scott JE. Elasticity in extracellular matrix “shape modules” of tendon, cartilage, etc. A sliding proteoglycan-filament model. J Physiol. 2003; 553:335–43. [PubMed: 12923209]
52. Lujan TJ, Underwood CJ, Henninger HB, Thompson BM, Weiss JA. Effect of dermatan sulfate glycosaminoglycans on the quasi-static material properties of the human medial collateral ligament. J Orthop Res. 2007; 25:894–903. [PubMed: 17343278]
53. Lujan TJ, Underwood CJ, Jacobs NT, Weiss JA. Contribution of glycosaminoglycans to viscoelastic tensile behavior of human ligament. J Appl Physiol. 2009; 106:423–31. [PubMed: 19074575]
54. Fessel G, Snedeker JG. Evidence against proteoglycan mediated collagen fibril load transmission and dynamic viscoelasticity in tendon. Matrix Biol. 2009; 28:503–10. [PubMed: 19698786]
55. Svensson RB, Hassenkam T, Hansen P, Kjaer M, Magnusson SP. Tensile force transmission in human patellar tendon fascicles is not mediated by glycosaminoglycans. Connect Tissue Res. 2011; 52:415–21. [PubMed: 21453063]
56. Liu X, Yeh M-L, Lewis JL, Luo Z-P. Direct measurement of the rupture force of single pair of decorin interactions. Biochem Biophys Res Commun. 2005; 338:1342–5. [PubMed: 16263082]
57. Rigozzi S, Müller R, Stemmer A, Snedeker JG. Tendon glycosaminoglycan proteoglycan side chains promote collagen fibril sliding – AFM observations at the nanoscale. J Biomech. 2013; 46:813–8. [PubMed: 23219277]
58. Zhang G, Young BB, Ezura Y, Favata M, Soslowsky LJ, Chakravarti S, et al. Development of tendon structure and function: regulation of collagen fibrillogenesis. J Musculoskelet Neuronal Interact. 2005; 5:5–21. [PubMed: 15788867]
59. Ansorge HL, Meng X, Zhang G, Veit G, Sun M, Klement JF, et al. Type XIV collagen regulates fibrillogenesis: premature collagen fibril growth and tissue dysfunction in null mice. J Biol Chem. 2009; 284:8427–38. [PubMed: 19136672]
60. Ricard-Blum S, Ruggiero F. The collagen superfamily: from the extracellular matrix to the cell membrane. Pathol Biol. 2005; 53:430–42. [PubMed: 16085121]
61. Veres SP, Harrison JM, Lee JM. Repeated subrupture overload causes progression of nanoscaled discrete plasticity damage in tendon collagen fibrils. J Orthop Res. 2013; 31:731–7. [PubMed: 23255142]
62. Fung DT, Wang VM, Andarawis-Puri N, Basta-Pljakic J, Li Y, Laudier DM, et al. Early response to tendon fatigue damage accumulation in a novel in vivo model. J Biomech. 2010; 43:274–9. [PubMed: 19939387]
63. Goh KL, Aspden RM, Mathias KJ, Hukins DWL. Effect of fibre shape on the stresses within fibres in fibre-reinforced composite materials. Proc R Soc A. 1999; 455:3351–61.
64. Folkhard W, Mosler E, Geercken W, Knörzer E, Nemetschek-Gansler H, Nemetschek T, et al. Quantitative analysis of the molecular sliding mechanisms in native tendon collagen – time-resolved dynamic studies using synchrotron radiation. Int J Biol Macromol. 1987; 9:169–75.
65. Knörzer E, Folkhard W, Geercken W, Boschert C, Koch MH, Hilbert B, et al. New aspects of the etiology of tendon rupture. An analysis of time-resolved dynamic-mechanical measurements using synchrotron radiation. Arch Orthop Trauma Surg. 1986; 105:113–20. [PubMed: 3718188]
66. Kastelic J, Baer E. Deformation in tendon collagen. Symp Soc Exp Biol. 1980; 34:397–435. [PubMed: 7256561]

67. Barenberg SA, Filisko FE, Geil PH. Ultrastructural deformation of collagen. Connect Tissue Res. 1978; 6:25–35. [PubMed: 149647]

68. Wang XT, Ker RF. Creep rupture of wallaby tail tendons. J Exp Biol. 1995; 198:831–45. [PubMed: 9244804]

69. Reese SP. Tendon fascicles exhibit a linear correlation between Poisson's ratio and force during uniaxial stress relaxation. J Biomech Eng. 2013; 135:034501.

70. Yin L, Elliott DM. A biphasic and transversely isotropic mechanical model for tendon: application to mouse tail fascicles in uniaxial tension. J Biomech. 2004; 37:907–16. [PubMed: 15111078]

71. Shen ZL, Kahn H, Ballarini R, Eppell SJ. Viscoelastic properties of isolated collagen fibrils. Biophys J. 2011; 100:3008–15. [PubMed: 21689535]

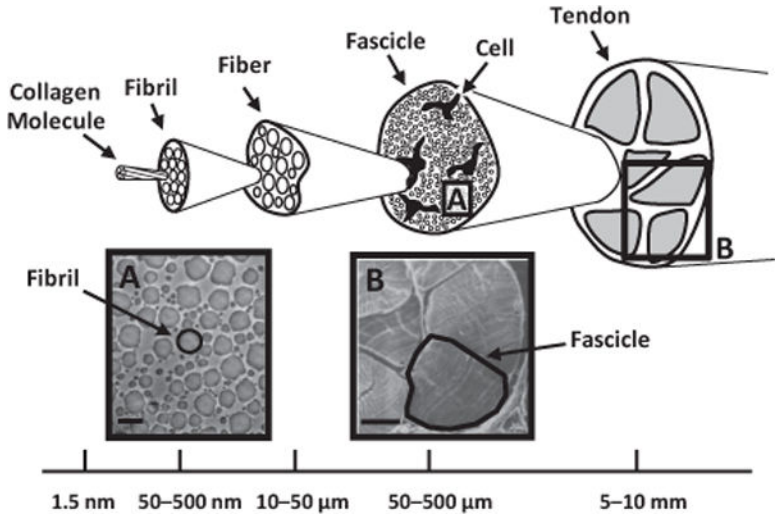


**Fig. 1.**

Collagenous hierarchical structure in tendon (adapted from Kastelic et al. [1]). Collagen molecules aggregate into extracellular structures called fibrils, which are the primary tensile load-bearing elements in connective tissues. In tendon, fibrils are highly aligned and form dense macroscopic subunits called fascicles. Also contained within each fascicle are cells whose extended processes loosely separate the fibrils into local partitions called fibers [2,3]. (A, B) Electron micrographs of fibrils and fascicles showing detailed views of corresponding regions highlighted in the hierarchical structure. Micrograph (B) is reprinted with permission from Rowe [2]. Scale bars: (A) 500 nm, (B) 100 μm.

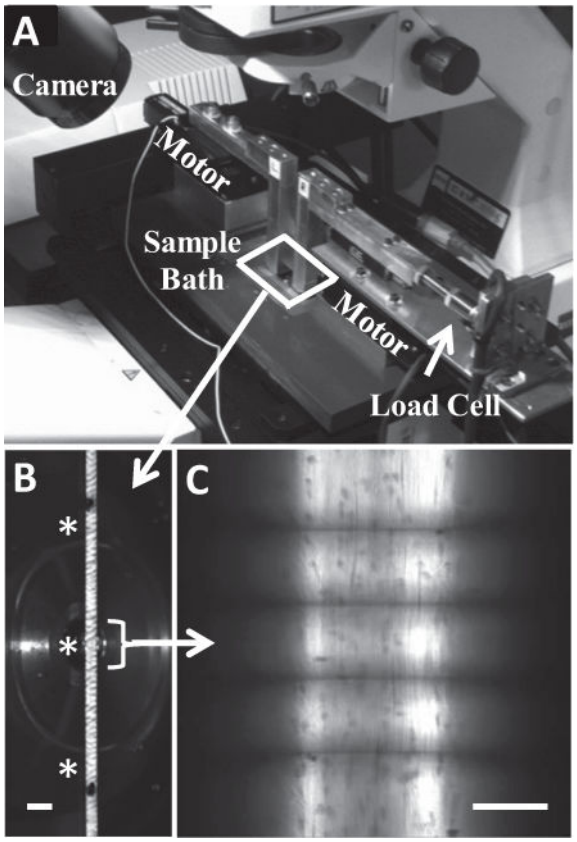


**Fig. 2.**

Experimental setup for multiscale tension testing. (A) Uniaxial tension device mounted on a confocal microscope. (B) Macroscopic image of a fascicle with ink marks used for measuring macroscale tissue strains. Asterisks mark the three locations of photobleached lines for microscale strain measurements. Scale bar: 1 mm. (C) Representative microscale image of photobleached lines taken with objective lens. Scale bar: 100 μm.

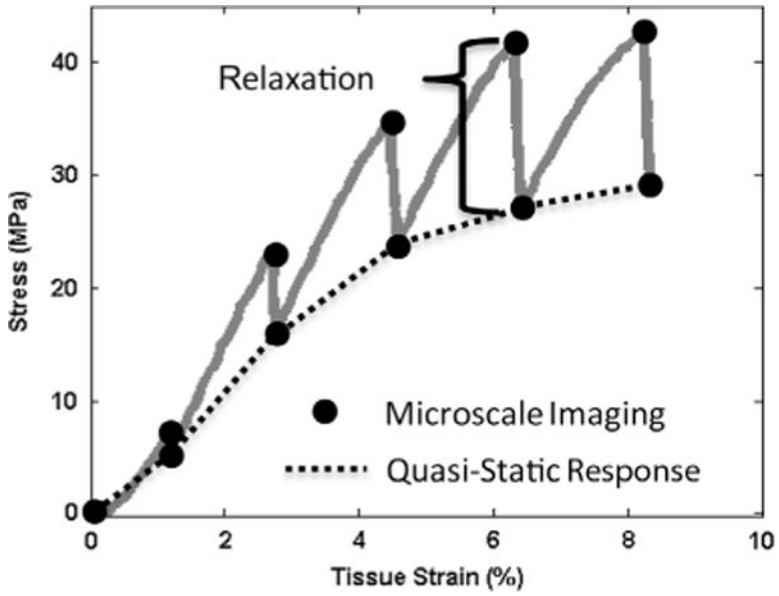


**Fig. 3.**

Representative plot of macroscale mechanical behavior with schematic of microscale imaging points and measurements of macroscale tensile properties (i.e. quasi-static tensile modulus and incremental percent stress relaxation).

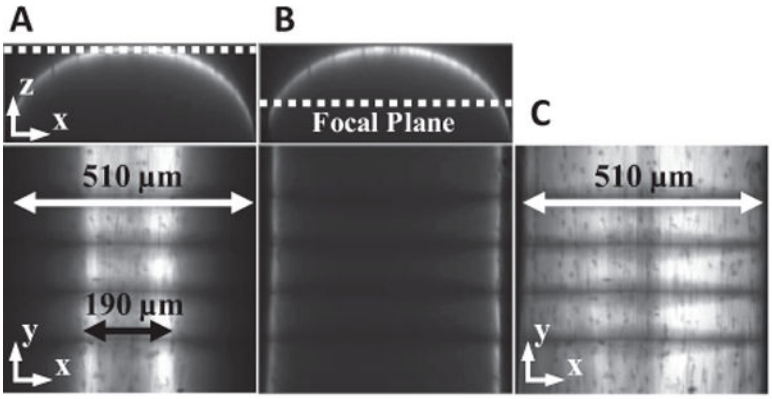


**Fig. 4.**

Production of single composite microscale image spanning the full tissue width. (A, B) Microscale images taken at a single focal plane capture only part of the full fascicle width (510 µm). (C) A single composite image covering the entire fascicle width can be produced by concatenating the information contained within each planar image.

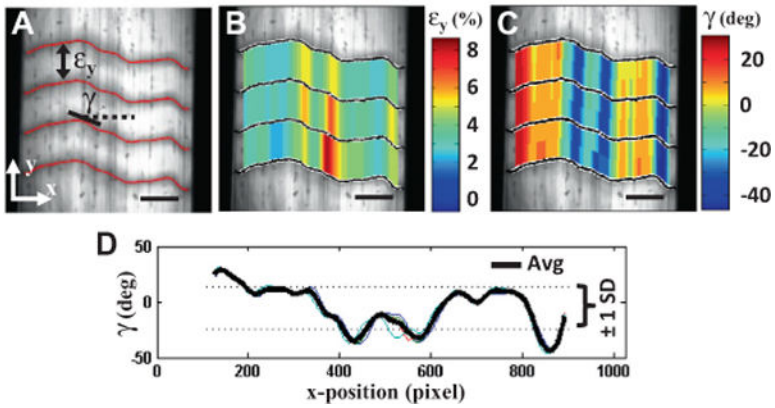


**Fig. 5.**

Measurement of microscale deformations. (A) Fibril strains ($\varepsilon_y$) and microscale shear strains ($\gamma$) were calculated from the displacements of photobleached lines. Representative 2-D plots of the (B) fibril strains and (C) shear strains measured at 10% grip strain. The fibril:tissue strain ratio was calculated by dividing the average fibril strain by the applied tissue strain. (D) The overall amount of interfibrillar sliding was quantified by the standard deviation (SD) of the shear strains averaged across the four photobleached lines. Scale bars: 100 μm.

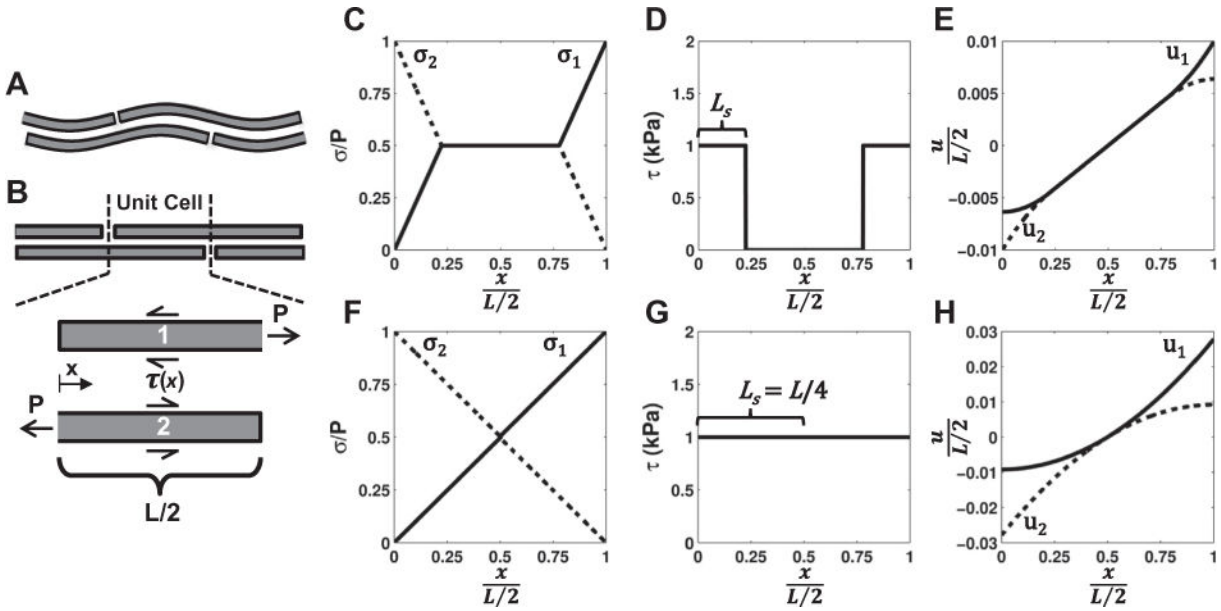


**Fig. 6.**

Construction of microstructural shear lag model. (A) The model consisted of a periodic array of discontinuous, staggered and crimped fibrils. (B) Once a unit cell was uncrimped, the fibrils began to bear load, which was transferred between fibrils through a perfectly plastic interfibrillar shear stress ($\tau(x)$). (C–E) Distributions of the (C) fibril stress ($\sigma$), (D) interfibrillar shear stress and (E) fibril displacement ($u$) produced by the model for low applied strains (e.g. $\varepsilon_{uc}$ = 2%). Note that the interfibrillar shear stress only occurs where there is relative sliding between fibrils (i.e. $u_1 \neq u_2$), which is initially isolated at the fibril ends. (F–H) At higher applied strains, the region of interfibrillar sliding ($L_S$) increases until the sliding and shear stress occur over the entire fibril length ($L_S = L/4$), maximally loading the fibrils. An increase in the tissue strain beyond this level will simply cause the fibrils to slide without further elongation.

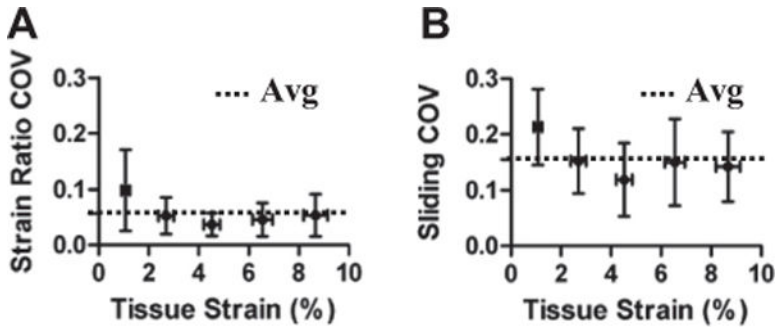


**Fig. 7.**

Low coefficients of variation (COV) for the (A) fibril:tissue strain ratio and (B) interfibrillar sliding demonstrate that these measurements are consistent along the sample length and accurately represent the microscale deformations throughout the tissue.

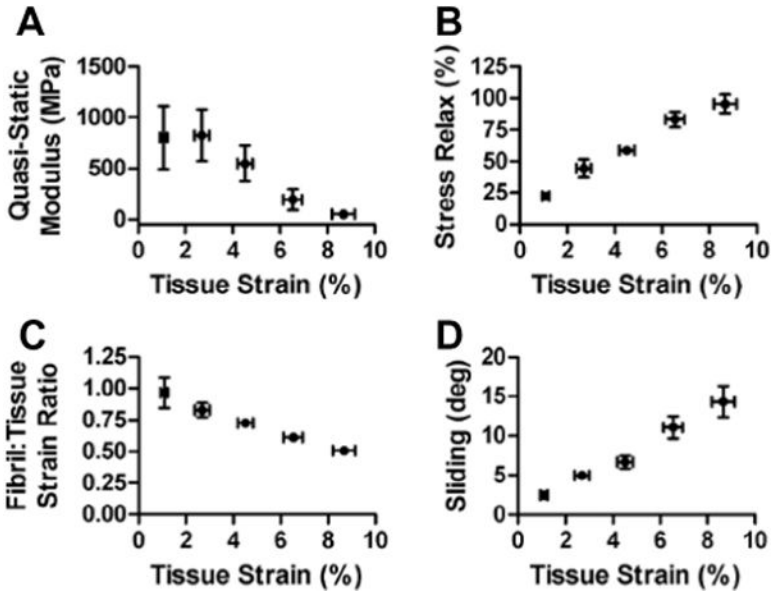


**Fig. 8.**

Multiscale tensile behavior of tendon fascicles. At the macroscopic length scale, tendon fascicles became (A) less stiff and (B) more viscous at greater applied tissue strains, which is typical for post-yield tensile behavior [33]. At the microscale level, concurrent (C) decreases in the fibril:tissue strain ratio and (D) increases in interfibrillar sliding suggest that fibrils are discontinuous, with the macroscale tissue strain resulting from the combination of fibril elongation and sliding.

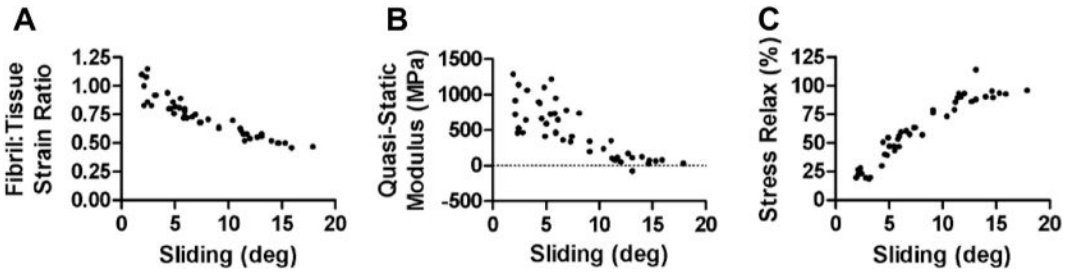


**Fig. 9.**

Relationship between fascicle macroscale mechanics and interfibrillar sliding. (A) The decrease in the fibril:tissue strain ratio with greater interfibrillar sliding suggests that relative sliding serves to unload the fibrils, which produces a (B) drop in the macroscale tissue modulus. These data suggest that interfibrillar sliding is responsible for the strain softening observed in the post-yield behavior of tendon fascicles. (C) A strong correlation between the macroscale stress relaxation and interfibrillar sliding suggests that sliding is associated with a viscous interfibrillar shear stress that transmits load between fibrils.

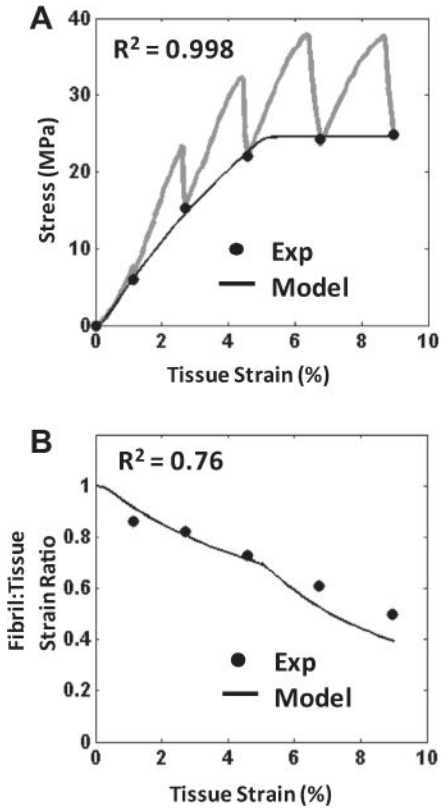


**Fig. 10.**

Representative plots of the model performance. (A) The model successfully fitted the quasi-static macroscale mechanics (●) ($R^2 = 0.996 \pm 0.003$), which was used to determine values for the model parameters. Note that the transient behavior during the strain ramps and stress relaxation are given by the gray lines. (B) While keeping the model parameter values fixed, the model also successfully predicted the fibril:tissue strain ratio ($R^2 = 0.74 \pm 0.18$). This ability to approximate the mechanics at both length scales validates the model assumptions and suggests that interfibrillar shear is the loading mechanism of the discontinuous fibrils in tendon fascicles.